Epoxy adhesive behaviour on ceramic surfaces in commercial optoelectronic assemblies

O. Williams#, C. Liu, D.P. Webb, P. Firth*

Mechanical and Manufacturing Engineering
Loughborough University, Loughborough, LE11 3TU

*Bookham Technology PLC, Brixham Road, Paignton, Devon, TQ4 7BE

#Email: O.Williams@Lboro.ac.uk

Abstract

Chemical and physical variability in the as-received state of aluminium oxide and aluminium nitride ceramic substrate materials used in optoelectronic modules currently leads to a process yield less than 100% when adhesives are used for assembly and interconnection. The phenomenon of epoxy bleed is a contributing factor to this yield and steps are not yet taken in the industry to control or inhibit the undesirable wetting.

Standard surface texture measurement techniques, XPS and contact angle measurements were implemented to characterise and compare commercial as-received samples. The quality controls currently in place are assessed and additional analysis methods in the QC stage are suggested for increasing yield. Commercially available conductive and thermally conductive adhesives, also used in optoelectronic module manufacture, were studied along with the surfaces.

In this work the surface property measurements, wetting observations and shear failure modes are compared and discussed. It was found that varying as-received surface properties did not affect adhesion strength between the adhesives and ceramics enough to induce an undesirable failure mode, although epoxy bleed distance varies dramatically with varying surface conditions.

Keywords

Epoxy/epoxides, ceramics, epoxy bleed

Introduction

The components in many modern optoelectronic modules are assembled using adhesives at greater spacing than optically necessary. Given the current trend towards miniaturisation in the optoelectronics industry [1], it is desirable to reduce the component spacing to allow for further reduction in the size of the module. This issue extends to many microelectronic applications in which adhesives are used for component assembly. One of the factors limiting reduction in component spacing is lack of control of the surface wetting behaviour of the epoxy adhesives on the ceramic sleds used as the optical bench. Good wetting is usually considered desirable to ensure strong and reliable adhesive joints. However, good wetting also increases the area of the joint fillet and hence reduces the potential to pack components more closely together. A further problem is variability in wetting behaviour and hence fillet size from batch to batch of the ceramic sleds. In extreme cases epoxy bleed occurs, where one or more adhesive components separate out before curing and spread widely across the ceramic surface, interfering with wire bonding processes and the application of subsequent adhesives.

The aims of the investigation described in this paper were firstly to understand the origin of the variability in adhesive wetting on ceramic sleds observed on the production line, and then to suggest cost-effective methods of reducing or eliminating it, particularly bleed. A subsidiary aim was to scope the possibility of reducing adhesive joint fillet sizes, without affecting the reliability of the optoelectronic modules. To achieve these aims the study was carried out on a representative range of different types of ceramic sled obtained from the

optoelectronic industry supply chain, in the condition in which they would be received by an optoelectronic module assembly plant. The results of surface characterisation of the as-received samples, of bleed measurements with epoxy adhesives used in optoelectronic assembly on as received and plasma cleaned samples, and of adhesion strength tests with the epoxies and ceramics, are reported here. Conclusions are drawn as to the alternatives for reducing variability in wetting behaviour and eliminating bleed.

Background

Aluminium oxide and aluminium nitride are popular substrate materials used in optoelectronic modules. Their low thermal expansion, dimensional stability and relatively high thermal conductivity make them ideal for use in high power applications. The similarity between the coefficient of thermal expansion (CTE) of Al_2O_3 ($9.5e^{-6}$/K), AlN ($5.6e^{-6}$/K), and silicon ($2.6e^{-6}$/K) means they are compatible materials with little reduction in reliability due to CTE mismatch. The CTE and thermal conductivity of the ceramics makes them suitable for use as substrate materials for laser transmitter modules where the laser diode requires good thermal draining. If the laser diode sees excessive temperature then the wavelength of the laser can be affected, jeopardising the functionality of the transmitter. An intermediate material is required for bonding the optoelectronic components to the ceramic substrate material, including the laser diode. Filled epoxy adhesives are used for this purpose. Epoxies are electrically and thermally insulative (thermal conductivity 0.2W/m/K), and so the adhesives used in the assembly line are filled either with silver, for electrical conduction, or boron nitride for thermal conduction. The use of

adhesives in the assembly of optoelectronic modules leads to a less than 100% process yield. One of the contributors to module failure is the uncontrolled spread of epoxy adhesive material over the substrate and interconnection features. However, optoelectronics manufacturers can only specify dimensions, tolerances and surface finish when purchasing ceramic substrate materials, not wetting properties. Different surface preparation methods are used by the ceramic manufacturers to achieve a specified R_a value. These include lapping, polishing, chemical etching and no surface preparation after sintering (as-fired). The different surface preparations are used in the optoelectronics assembly line with little understanding of the effects of the treatments on the adhesive wetting and the bond strengths.

The manufacture of the substrates is done in two stages, typically by different companies. Ceramic tiles are produced from a slurry and sintered into a polycrystalline solid with a grain size dependant on the application and manufacturer. The same company typically performs the surface treatment of the ceramics also. A second company dices the ceramic tiles and is the direct supplier to the optoelectronic manufacturer. A number of cleaning processes are included in the cutting process before a final firing at ~850°C in air. Substrates are typically shipped and stored in polymer waffle packs.

The surface chemical as-received state of the ceramic materials is not characterised by the optoelectronics manufacturer, and is uncontrolled in the assembly process, as substrates may or may not be subjected to further

cleaning. It is therefore a source of variation in the behaviour of adhesives on the ceramics, and in the quality of the adhesive joints formed.

The surface preparations used in the industry are usually quantified with R_a, R_t and R_z roughness parameters. However, for the purpose of this study a roughness factor was needed which could be directly related to wetting and adhesion. The Wenzel roughness factor was chosen as it makes frequent appearances in the literature as a roughness parameter which can be linked directly to wetting and adhesion [2]. The Wenzel roughness factor is the ratio of the actual surface area to the planar surface area, i.e.; a dimensionless parameter where a value of exactly one constitutes an ideal, perfectly flat surface with no deviation from the plane, and values greater than one correspond to real surfaces.

The relationship between roughness and contact angle is given by the Wenzel model to be:

$$r\cos\theta = \cos\phi \qquad (1)$$

Where ϕ is the apparent (measured) contact angle, θ is the ideal contact angle on a perfectly flat surface and r is the Wenzel roughness factor. This relationship predicts that for an intrinsic contact angle above 90° roughness will give an apparent increase in contact angle, and reduction in wetting. Whereas for a true contact angle below 90° roughness will act to decrease the contact angle and increase wetting. This relationship suggests that epoxy bleed could be affected by the roughness of the substrate material. Where it

occurs the degree of epoxy adhesive bleed has also been linked to substrate composition, contamination and surface energy [3,4].

Theories of wetting and adhesion suggest resin bleed could be controlled by surface texture alone [5], produced by mechanical processes which are already used in the production of the ceramic sleds that form the component substrates in optoelectronic modules. Surface texture or roughness on the nanometre scale is one of the most important factors determining the strength achieved by an adhesive bond. This can be because of mechanical interlock effects, but also because increased roughness can increase the area of intimate contact available for inter-material physical or chemical bonds [6]. By changing the surface texture of the substrates the actual bond area will change [7], whilst the apparent bond area remains constant. However it should be noted that attempts to control the epoxy resin bleed by means of surface texture could render the bond strength unacceptably weak [5]. Poor wetting of the adhesive on the substrate, and a high adhesive viscosity, could result in formation of air pockets at the interface [8] and a reduction in the actual bond area. A scientific approach to engineering surface wetting of the adhesive therefore requires separation out of the surface energy and surface texture effects of surface treatments.

Methodology

The ceramic sleds used in the study had undergone a variety of surface texture modifying treatments typically applied by suppliers to meet the R_a specified by the customer. The surfaces of the sleds were characterised for

surface texture, chemistry and wetting properties, in the as-received state. Several different methods of measuring surface texture were compared to identify the one most suited to the samples. Two different kinds of commercial epoxy-based adhesive that are also used for optoelectronic assembly were obtained and used in shear tests with the sleds. The degree of bleed of the epoxies on the ceramic surfaces was also measured. To separate out the relative influences of surface texture and surface texture, bleed measurements were also made on sleds which had been cleaned in an oxygen plasma.

Experimental Details

Sets of rectangular alumina and aluminium nitride ceramic sleds, of area 5.5mm×16mm and thickness 1mm, were bought from a commercial supplier to the optoelectronics industry. The surface preparations of the sleds were polished, lapped, as-fired, polishing followed by light etching, and polishing followed by heavy etching, as listed in

Table **1**. The R_a and R_T values given by the supplier for the samples had been obtained using a Mitotoyo Surftest SJ-400 surface contact probe with a 5μm tip radius.

The surface textures were subsequently characterised at Loughborough University using atomic force microscopy (AFM) measurements in tapping mode. The Wenzel roughness factor r and R_a were calculated from the data. White light interferometry (WLI) was also used to obtain values for R_a.

The chemical composition of the surfaces was measured using X-ray photoelectron spectroscopy (XPS), and the wetting characteristics by water and diiodomethane equilibrium sessile drop contact angle measurements on a contact angle goniometer. Surface energies were calculated from the contact angle measurements using the Owens Wendt Kaeble method. At least nine contact angles were recorded for each liquid on each surface from three samples. The Owens Wendt Kaeble method was chosen due to the expectation of a wide range of surface energies.

Application of adhesive spots to the sleds for bleed measurements and tensile tests was by dispensing from a syringe using a cylindrical needle 0.56mm in diameter. Tensile test pieces were prepared in a single lap joint configuration using commercial silver filled (H20E) and boron nitride loaded (930-4) epoxy adhesives, manufactured by Epo-Tek. The mating sled was mounted on to the adhesive spot using a jig that aligned the sleds and maintained a bond thickness of 30μm. All adhesives were handled, prepared and cured according to the manufacturer's instructions. The H20E adhesive components were combined in a 1:1 ratio by weight and the 930-4 adhesive components were combined in a ratio of 100:3.3 resin to curing agent ratio by weight, each measured to an accuracy of 0.01g. The adhesives were mixed thoroughly for 5 minutes. It was ensured that the adhesives were used within their pot lives of 24 hours, usually within 30 minutes of mixing. The adhesives were cured in an oven at 150°C for 30 minutes. The joints created varied in diameter from 1.8 mm to 4.3 mm, so the diameters were measured after failure in an SEM as described below. Some joints were subjected to thermal cycling from -40°C

to +80°C, with a twenty minute transition and ten minute dwell time, for two days. The adhesive joints were tested to the point of failure under shear loading using the compression function of an Instron micro tensile test machine. The compressive extension was controlled at a constant rate of 0.001mm/s whilst the applied load and extension were recorded. The fracture surfaces were examined by scanning electron microscopy (SEM) and profiled with an optical surface metrology system; Talysurf CLS 2000, to determine the failure mode. The joint areas for the shear stress calculation were taken to be the apparent areas of the fracture surfaces from the SEM images. A reference artefact was used to calibrate the measurements. For measurement of bleed from AFM images the bleed distance was taken to be the maximum perpendicular distance from a tangent to the adhesive spot that the material spread.

Plasma cleaning for removal of surface contamination consisted of one minute of treatment in a 300 W oxygen RF (13.56 MHz) plasma at a flow rate of 100 sccm. Removal of surface contamination was confirmed using diiodomethane and water contact angles, within 1 hour of treatment, to calculate a figure for apparent surface energy. AFM profiling before and after treatment confirmed that there was no observable effect on the surface topology.

Results

Surface Texture Analysis

From

Table **1** it can be seen that as fired samples (4-6 and 8) show a large range of roughness (0.05 μm ≤ Ra ≤ 0.85 μm), probably due to variation in the grain size of the ceramic in the green state prior to sintering. The granular texture of the as fired surfaces can be seen in the 3D AFM plot in Figure 5 for sample 8 (A_2O_3 as-fired, R_a 0.05 μm). The large variation in as-fired surface textures is one reason for a manufacturer to specify a mechanical or mechanical chemical surface preparation to the sleds to reduce manufacturing variations due to surface texture variation. To attempt to determine whether R_a gives sufficient information to allow this source of manufacturing variation to be controlled, white light interferometry and an AFM were also used to characterise the surface textures. The AFM gives the additional capability of producing a value for the Wenzel roughness ratio r. A comparison of R_a measured by the different methods plotted versus r is given in Figure 1.

On average (mean of the ratios) R_a by WLI is twice that by AFM. This is probably due to measurement artefacts in the WLI data. The 3D surface plots show multiple steep sided fissures which are not visible in AFM. The artefacts are probably caused by multiple reflections from the surface features which increase the length of the light path. Evidence for this suggestion is provided by the high frequency of the occurrence of the fissures in the profiles and their equal depth. In addition there is a high frequency of missing data in the profiles, probably due to the incident light angles being such that the light is not returned to the sensor. These issues have been documented in the literature [9].

The mean ratio of R_a by the stylus instrument (Surftest SJ-400) to that by AFM is around 1.3 (single anomalous data point at very low R_a ignored, stylus: AFM value of 25 at r=1.002). Since both methods are surface contact the closer correlation is unsurprising. However there are reasons to prefer the AFM measurements. In Figure 1 it can be seen that R_a by any method is not strongly correlated with r until R_a>0.2 μm. This shows that the AFM is picking up structure relevant to wetting in the surface texture at low R_a that is not reflected by that index. The major limitation of the AFM for assessing surface texture application is its inability to analyse large areas, and so properties such as flatness cannot be determined. However for adhesive flow micro and nanoscale roughness is likely to be more important. Other reasons for preferring the AFM are that profiles are measured along an outwards and a return stroke along the same line of travel. This gives added reliability to the measurements because the tracking of the two directions can be compared. The AFM used in tapping mode allows precise control of the pressure the tip exerts on the surface.

A potential reason for the anomalous R_a ratio obtained with the stylus instrument at low roughness (stylus: AFM value of 25 at r=1.002) is the nature of the situations in which the measurement methods are performed. The AFM is insulated against vibration and air flow whilst the portable stylus instrument has no means of filtering background vibration and atmospheric effects. The vulnerability of the stylus instrument to vibration could define its measurement limit, the point at which the effect of the surface upon the stylus is exceeded by the effect of noise.

An interesting result obtained with the AFM can be seen in Figure 4 for a polished Al_2O_3 surface (sample 9), which shows a 2D height plot. Despite the polishing a grain structure is still apparent. This is probably due to different hardnesses of the material across the surface. Intergranular material and grains with different crystalline orientations have been removed differing extents. This implies sharp height boundaries which may provide good keying features for adhesive joint formation.

Sample Surface Chemical and Contact Angle Characterisation

Surface chemical characterisation of the sleds was carried out by XPS, while the wetting characteristics were determined by contact angle measurement. The XPS elemental quantifications from broad scans are listed in Table 2. The major constituents of the AlN surface signal after aluminium and nitrogen were primarily carbon and oxygen, suggesting the presence of organic molecules, probably atmospheric or other contamination. High energy, clean surfaces such as the ceramics studied have a tendency to adsorb organic films upon exposure to air [5], the composition of which is determined by the atmosphere the surfaces are subjected to. The spectra of the Al_2O_3 indicated the presence of trace amounts of group 1 and 2 metals (calcium, sodium, magnesium) along with up to 14% silicon. The silicon is present on the surface regardless of surface preparation method, while the “as fired” samples exhibit a comparable surface composition of trace elements to those which have undergone further processing. It is difficult to determine the origin of these elements due to the commercial nature of the samples. The magnitude

of the signal from the group 1 and 2 metals is closely related to the purity of the samples as reported by the suppliers; those which were over 99% pure have only trace amounts of these elements present, whilst those 96% pure showed presence of up to 3%. The correlation with purity and insensitivity to surface treatment suggests that the trace elements form part of the material composition.

Figure 2 shows a plot of surface carbon percentage against r, showing that there is evidently no correlation. The two very high carbon percentage data points are for the etched AlN sleds, suggesting that either the chemical etch provides a clean high energy surface for the adsorption of higher levels of organic contamination, or that it leaves behind residues on the substrate surface after drying. There is also no evident correlation between the surface energy calculated from the contact angle measurements and r, as can be seen in Figure 5. The very high energy AlN surface (72 mJ/m^2) in Figure 5 is the lapped sample (number 7). The surface carbon content of this sample is not particularly low at 21.1%, so the low contact angles seen may be due to the high roughness (r of 1.63).

The lack of correlation between the surface energy calculated by wetting measurements and surface roughness is surprising in view of the well known effects of roughness on contact angles [2]. However, there is a clear correlation between surface energy and surface carbon visible in Figure 6, with surface energy decreasing with increasing carbon content for both AlN and Al_2O_3, apart from the anomalous result for sample 7 already noted, as seen in other work [4]. Since in principle both roughness and surface contamination affect wetting, it would therefore appear that the variation in carbon content is large enough to mask any effect of roughness on the contact angles in Figure 5 apart from the very rough lapped AlN (sample 7), while the roughness variation is not large enough to disturb the trend seen with carbon percentage in

Figure 6, again excepting sample 7. It is worth noting that the Ra value given by the supplier of 0.75 μm for sample 7 was not the highest in the sample set, while the value of r determined by AFM was the highest by some margin (next highest sample 5, r 1.35, Ra 0.61μm; highest Ra value sample 6 at 0.85 μm but r only 1.23). Wenzel's parameter r is therefore a better predictor of wetting than Ra with this sample set.

Bond Strength Analysis

Cohesive failure is the failure of a bond through the adhesive and is considered the failure mode which occurs in an ideal bond for it constitutes evidence that the adhesive has adhered to the adherend [6]. The indicator of cohesive failure in this case is that there are equal amounts of adhesive remaining on both the adherend surfaces. Figure 7 shows that equal amounts of adhesive remained on each surface of both rough and polished samples following shear failure (failed boron nitride filled adhesive spot, measured with a Talysurf CLI 2000).

Measurements were made on all failed joints and it was seen that all bonds underwent cohesive failure in the adhesive, and that therefore no inferences can be drawn as to the effects of the surface energies and textures on bond strength.

Further evidence for cohesive failure comes from the proportional relationship observed between the measured shear strength and measured bond area. In

Figure 8 it can be seen that the constant of proportionality is dependent on the choice of adhesive, and independent of surface type or treatment.

The near constant slope and instantaneous failure seen in the load vs extension curves for the tensile testing suggests the joint underwent elastic deformation followed by brittle fracture. SEM images of the failed adhesive surfaces supported this, for they showed no signs of plastic deformation and the topography of the adhesive consists of sharp jagged profiles typical of brittle failure. The jagged nature of the surface topography in the SEM images is consistent with the Talysurf profiles in Figure 7. The SEM images of the failed bonds also show failure occurred entirely though the adhesive.

The bond strengths were not detrimentally affected by thermal cycling, Figure 9 shows the same correlation between shear force and bond area as seen with the samples which were not cycled, along with comparable shear force values. The failure modes are comparable to those of the bonds which were not cycled. Figure 9 also shows the silver filled adhesive has become stronger after thermal cycling, a possible reason for this is that the adhesive continued to cure at the elevated temperatures in the cycles. Manufacturer's data gives a 80°C cure time of 90 minutes for the silver filled epoxy and 6 hours for the boron nitride filled epoxy, supporting this theory.

Higher magnification SEM images of the failed silver filled epoxy bonds showed the failure occurred along the boundaries between the epoxy adhesive polymer and the silver flakes. The images suggested that the weak

interface is that between the components of the adhesives, and as the other evidence supports, not between the adhesive and the ceramic surfaces.

Epoxy Bleed

The resin bleed phenomenon appears not to be exclusively related to the contaminants found to be present. Figure 10 shows examples of minimal and pronounced bleed respectively on surfaces which were found to have an equal degree (21%) of carbon contamination. The pronounced bleed occurs on the lapped surface (r 1.63), rather than the polished surface (r 1.00). It was therefore hypothesised that the bleed materials wetting performance might be sensitive to both topography and composition. For the most part the very thin bleed films were not highly visible optically, so a scanning electron microscope (SEM) in secondary electron (SE) mode was used to measure their extent. An example of minimal bleed is shown in Figure 11(a). The bleed is visible as a dark band surrounding the bulk adhesive with high contrast to the surrounding area and with reduced filler content compared to the bulk. Figure 11(b) shows pronounced bleed at a much reduced scale. The bleed can still be distinguished as a dark area around the central sessile drop. The topic of contrast in SE images is a complex one. However it seems likely the contrast between the bleed and bulk is due to the higher atomic number of the filler in the bulk increasing the secondary electron yield from that region. See for example Sakai et al [10]. Of the samples listed in

Table **1**, pronounced epoxy bleed was witnessed on 2 samples both of which had comparatively low carbon contamination and comparatively high surface roughness, samples 5 and 7(r = 1.37, 1.63 respectively, bleed distance

1.1mm, 2.2 mm respectively). Minimal or no bleed was observed on samples 1-4 and 8-10, samples 3 and 12, both of which were polished (r = 1.0024, 1.0021 respectively), showed no bleed from the silver filled adhesive, and <10μm of bleed from the boron nitride filled adhesive.

In order to separate out unambiguously the influences of surface roughness from that of surface contamination/surface energy, the samples were cleaned using an oxygen plasma to reduce the variation in surface contamination among samples. Oxygen plasma was chosen for its effectiveness in reacting with carbon based molecules and its slow etching rate for the ceramics of interest. Contact angle measurements on all samples which underwent this treatment gave apparent surface energies in excess of 70mN/m. This suggests removal of the majority of contamination, although the apparent surface energy is not high enough to denote complete removal [11]. The upper measurement limit of the surface energy is defined by the surface tensions of the liquids used, if the surface energy exceeds the surface tension of the test liquid then a stable contact angle is not formed and the surface energy cannot be estimated with the contact angle method. Low contact angles <10° were witnessed with water following plasma treatment, this indicated highly polar surfaces which are very near the useful limit of water as a test liquid.

The dispersive component of the surface energy was unchanged by the plasma treatment, whilst the polar component increased to 50mN/m (standard deviation 1.03), for all samples. This supports the suggestion that the main

effect of the plasma exposure is to remove carbon based contamination, thus reduced the hydrophobicity of the surfaces. While the contact angle technique may not be capable of resolving any remaining differences in total surface energy among samples, XPS analysis of the plasma cleaned samples showed a relative carbon percentage of 12% on all samples. It therefore seems justifiable to consider the surfaces to have been chemically homogenised, allowing the differences in bleed behaviour described below to be attributed solely to differences in surface roughness.

Following the plasma clean the adhesives were applied as sessile drops to the sample surfaces within 1 hour of cleaning and cured as before. Removal of contamination results in all surface/adhesive combinations exhibiting bleed visible to the naked eye, except the polished surface 9 with the silver filled adhesive and the polished surface 3 with both adhesives. Figure 12 shows bleed distance plotted versus the AFM measured Wenzel ratio value for both substrate and adhesive materials and a roughly linear correlation can be seen. The alumina data points show more scatter about the linear trend line. It can also be seen that the boron nitride filled adhesive consistently bleeds further at each roughness value for both ceramic types than the silver filled adhesive. This shows that the bleed distance is partly affected by the adhesive formulation, probably because different adhesive additives or the filler properties either inhibit or encourage epoxy bleed. Further investigation of the effects of adhesive composition was beyond the scope of this work, partly because the commercial nature of the adhesives used meaning that the ingredients were not identified. However the influence of the ceramic surface

on the bleed distance, is far stronger than that of the adhesive type. The result is possibly due to capillary action, which is known to extend to liquid spreading over surfaces [12].

It can be seen in Figure 13 that the dispersive component of the apparent surface energy is strongly linearly correlated to the roughness, irrespective of surface material. However the total variation in the dispersive component of surface energy (2%) is much smaller than the observed total variation in bleed distance (68%). It therefore seems likely that the effect is due to the influence of roughness on the contact angles measured using the test liquids, from which the surface energy is calculated, and hence that the bleed distances are indeed being determined solely by the ceramic surface texture after plasma cleaning, for each epoxy type.

Conclusions

Both adhesives exhibited unacceptable bleed distances on most of the plasma cleaned ceramic surfaces, but on only two of the uncleaned surfaces. Adventitious surface contamination is therefore an integral part of the product quality of optoelectronic module assemblies. It is undesirable that such an important parameter is completely uncontrolled by either part specifications or goods inwards checks. A simple qualitative wetting test with a suitable liquid could probably be made the basis of the necessary control if considered along with the roughness measurements which are currently supplied with the ceramics.

For the adhesive/adherend systems investigated all joints failed cohesively, so that the mechanical surface preparation and surface chemistry had no influence on measured bond strength. This means that there is scope for engineering the surfaces in the study to reduce bleed without affecting bond strength or thermal fatigue resistance. This engineering will be the subject of further work.

The level of carbon based contamination was found to be a much stronger influence on wetting of the ceramics than surface texture with as received samples. However, once the contamination was removed it was clear that the surface texture, quantified as the Wenzel roughness factor, has a large effect upon the promotion or resistance to epoxy bleed.

Apparent surface energy alone is thus not sufficient information to determine the degree of epoxy bleed on a surface. This work has highlighted that surfaces of very low roughness and high surface energy can still resist epoxy bleed, and that surfaces of equal apparent surface energy but different roughnesses show different bleed behaviour. If the components of apparent surface energy are considered separately a clear linear correlation can be seen between the dispersive component and the bleed distance. The bleed distance is also linearly correlated with the AFM Wenzel ratio (r) value, indicating that the surface texture is directly linked to the measured dispersive component of surface energy. It can therefore be concluded that surface texture does have a direct effect upon the bleed distance, once contamination

is removed. This gives rise to the possibility of varying surface texture as a means of epoxy bleed control.

Portable hand-held surface roughness measuring machines are not, in this case, particularly suited to giving an accurate representation of a ceramic surface, due to the feature size being such that it is not penetrable by the probe. For a smooth surface this is especially apparent as the surface has been machined to give the smallest feature size possible.

Light based methods of surface measurement are also not suitable for these ceramic samples, for the crystal angles and steep angles of the topography create missing data points due to the incident angle being such that the light is not returned to the sensor. Steep fissures also appear to be present using this method, but their nature and absence with other analysis methods suggest this is a phenomenon of the method and not an actual surface feature. The limited effectiveness of these surface analysis methods suggests that manufacturers should adopt high resolution stylus profiling methods, such as AFM, for quantifying the roughness of ceramics.

Acknowledgments

The authors would like to thank Andrew Walker of LEW Techniques Ltd for supply of ceramic materials.

References

1. Hall, J.; Edge, C.; Randle, F.; Pope, S.; Fraser, J.; Loosley, J.; Kimber, E.M.; Firth, P “Integrated tunable transmitters for 10Gb/s long-haul DWDM applications” 53rd Electronic Components and Technology Conference, New Orleans May 27-30 2003 Page(s):796 – 800

2. Wenzel, Robert N. Surface Roughness and Contact Angle *J. Phys. Chem.*, 53, 9, 1466 - 1467, 1949, 10.1021/j150474a015

3. Hsiung, J.C. Pearson, R.A. Lloyd, T.B. “A surface energy approach for analyzing die attach adhesive resin bleed” Journal of adhesion science and technology 2003 Vol. 17 Issue no. 1 pp 1-14

4. Burmeister, M. “Elimination of epoxy resin bleed through thin film plasma deposition” Proceedings of SPIE--the international society for optical engineering 2003 Vol. 5288 pp 780-785

5. Surface analysis and pretreatment of plastics and metals / edited by D.M. Brewis. -- London : Applied Science, 1982

6. Pocius, Alphonsus V. Adhesion and adhesives technology : an introduction / Cinncinati, Ohio : Hanser Gardner, 2002.

7. Lawrence, J. (Jonathan), Li, L. (Lin), Laser modification of the wettability characteristics of engineering materials / London : Professional Engineering, 2001.

8. A. B. D. Cassie and S. Baxter, Wettability of porous surfaces, Trans. Faraday Soc. , 1944, 40, 546 - 551

9. Pavliček, P. Hýbl, O. White-light interferometry on rough surfaces--measurement uncertainty caused by surface roughness Applied Optics, Vol. 47, Issue 16, pp. 2941-2949 2008

10. Y. Sakai, T. Yamada, T. Suzuki, T. Ichinokawa, Contrast mechanisms of secondary electron images in scanning electron and ion microscopy, Applied Surface ScienceVolumes 144-145, , April 1999, Pages 96-100.

11. M. L. Guzman-Castillo, X. Bokhimi, A. Rodriguez-Hernandez, A. Toledo-Antonio, F. Hernandez-Beltran, J. J. Fripiat, The surface energy of quasi-amorphous [gamma] alumina calculated from the temperature of the [gamma]-->[alpha] transition, Journal of Non-Crystalline Solids, Vol329, Iss 1-3, November 2003, Pg53-56

12. Starov, V. M. Velarde, Manuel G. (Manuel García) Wetting and spreading dynamics / Boca Raton, Fla. ; London : CRC/Taylor & Francis, 2007.

Table of figures

Tables

Sample number	Material	Preparation	Ra (μm)	Rt(μm)
1	AlN	Polish + light etch	0.06	1.3
2	AlN	Polish + heavy etch	0.08	2.7
3	AlN	Polished	0.04	1.9
4	AlN	As fired	0.17	2.1
5	AlN	As fired	0.61	4.9
6	AlN	As fired	0.85	7.2
7	AlN	Lapped	0.75	8.2
8	Al_2O_3	As fired	0.05	0.5
9	Al_2O_3	Polished	0.02	0.4
10	Al_2O_3	Lapped	0.45	4.0

Table 1 Measured surface properties of as-received materials.

	Relative atomic percentage							
Sample	Al	O	N	C	Si	Mg	Ca	Na
1	23.5	37	4	35.6	0	0	0	0
2	28.6	25.3	13.7	32.5	0	0	0	0
3	31.7	39.2	9	20.1	0	0	0	0
4	28.9	42.4	6.2	22.6	0	0	0	0
5	30.4	42.5	5.5	21.6	0	0	0	0
6	33.4	44.6	5.2	16.8	0	0	0	0
7	30.1	42.8	6	21.1	0	0	0	0
8	23.1	44	0	18.2	12.3	0.9	0.5	1
9	28	40.2	0	21.2	8.8	1.2	0	0.6
10	20.1	39.4	0	21	14.2	3.2	2.2	0

Table 2 Relative atomic percentages of the elements present on the ceramic substrates, measured using XPS.

Figures

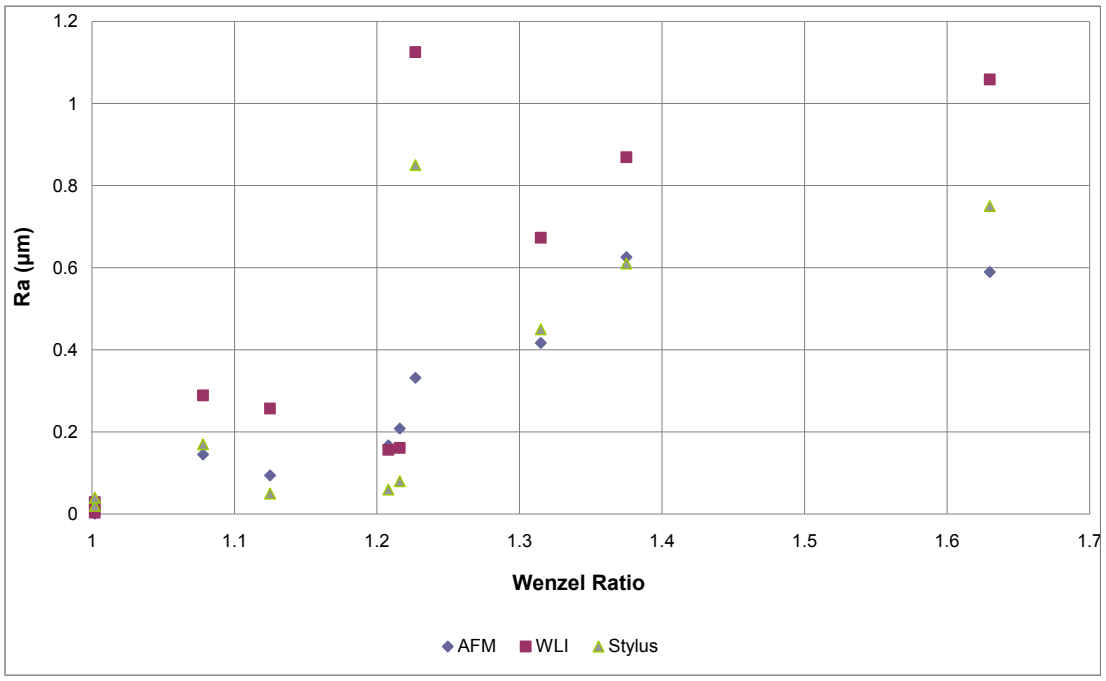

Figure 1 Comparison of Ra roughness values produced by AFM, WLI and stylus profiling to the Wenzel ratio produced by AFM.

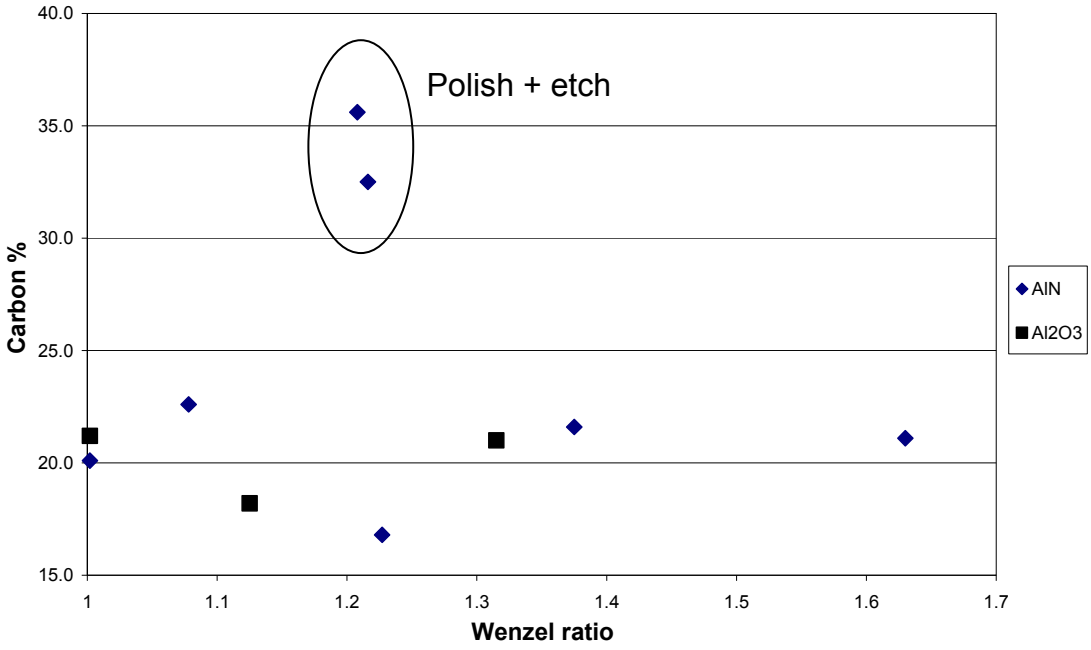

Figure 2 Comparison of Wenzel ratio to relative carbon percentage as measured with XPS

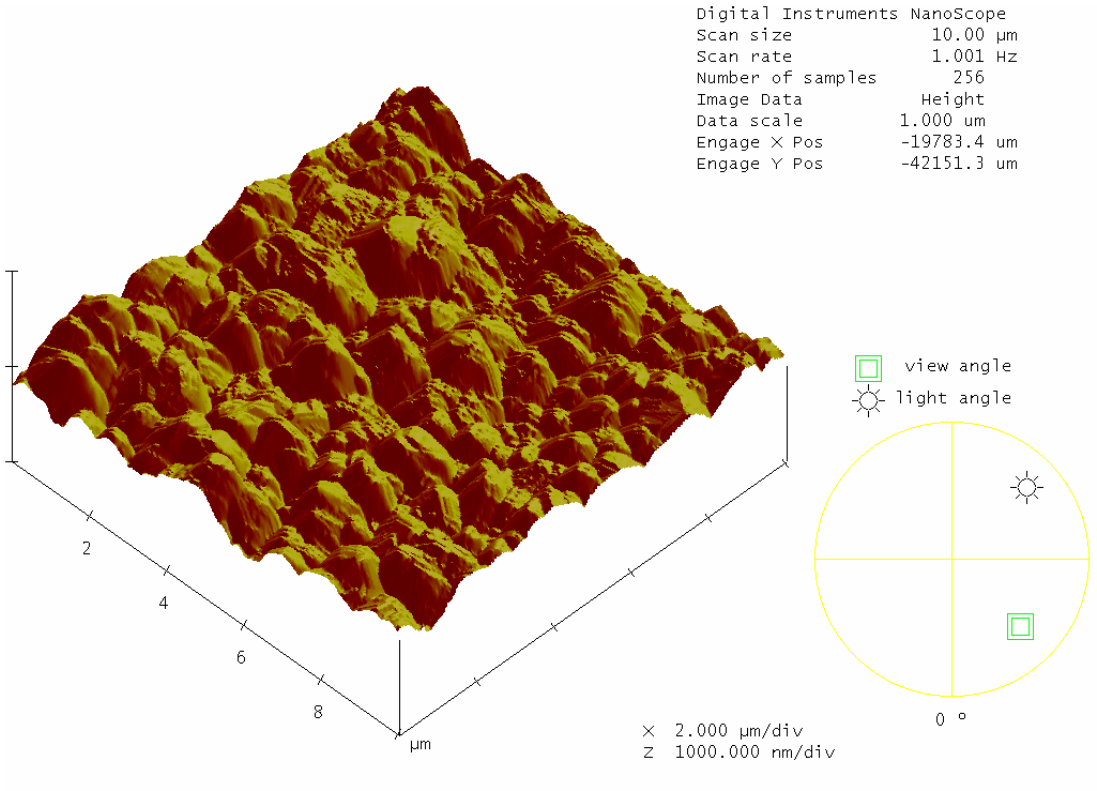

Figure 3 AFM 3D morphology representation of sample 8 Rt value 0.791µm

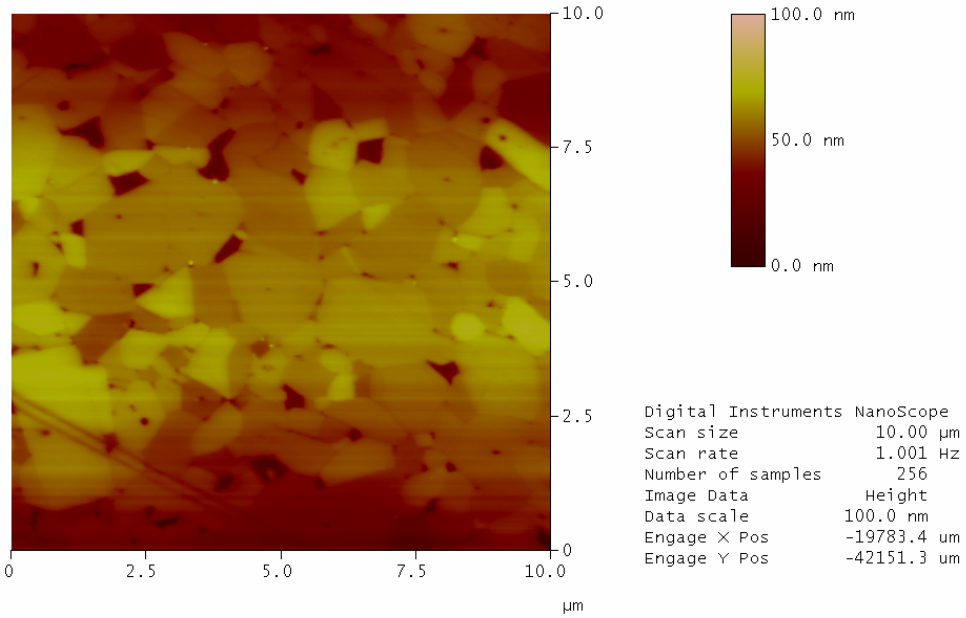

Figure 4 AFM 2D representation of 3D morphology of sample 9

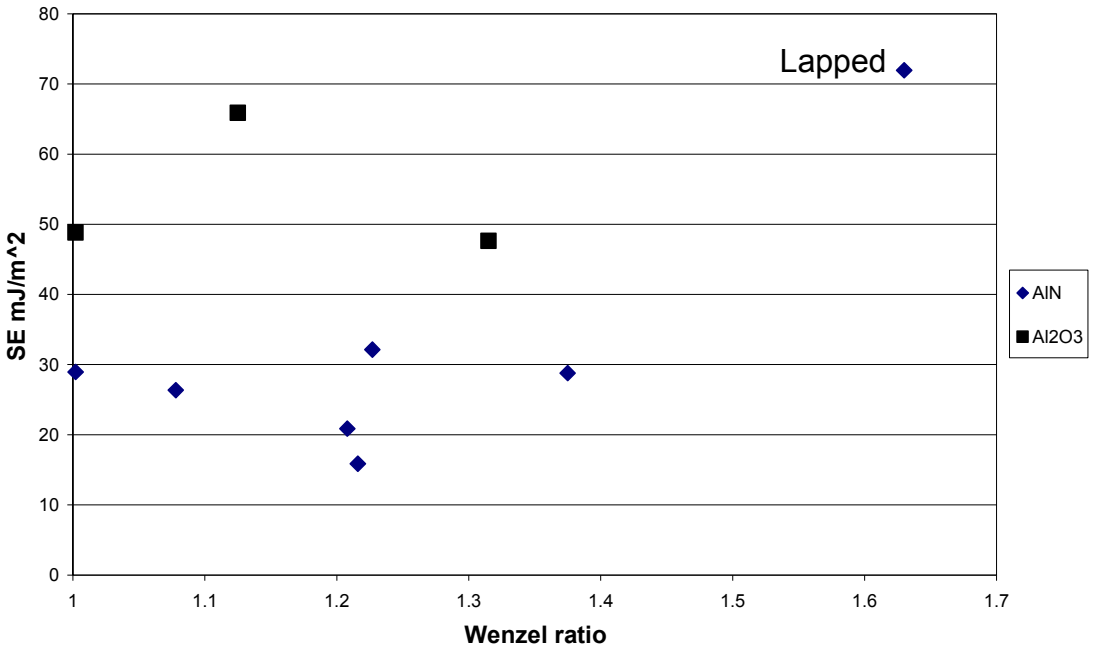

Figure 5 Plot of apparent surface energy (according to Owens-Wendt) against the Wenzel ratio.

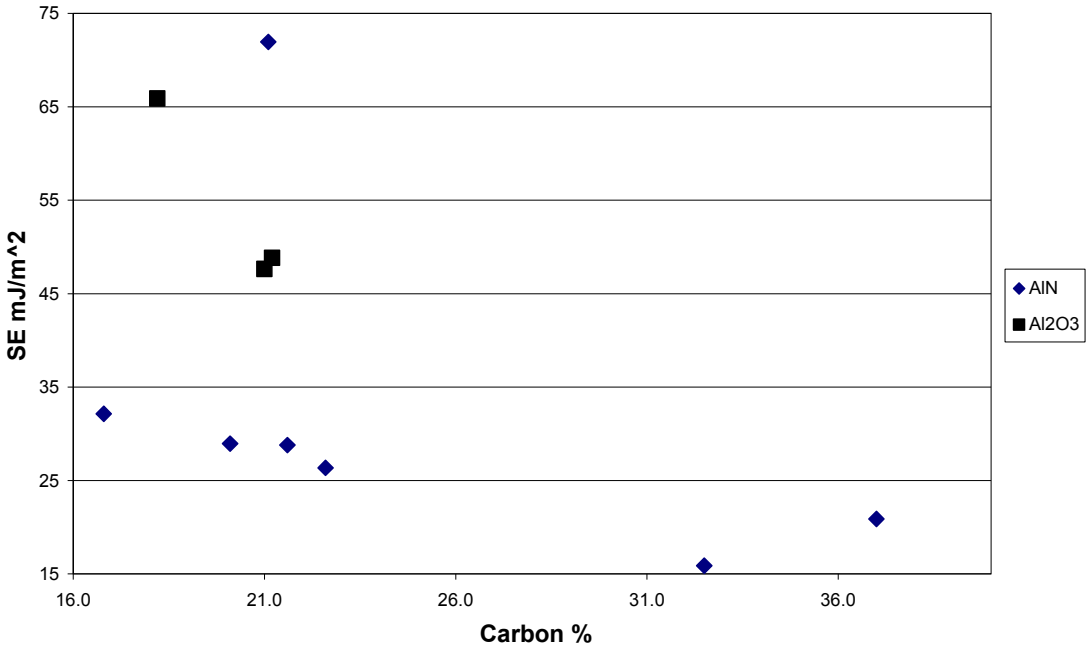

Figure 6 Plot of surface energy (according to Owens-Wendt) against relative atomic carbon percentage as by XPS.

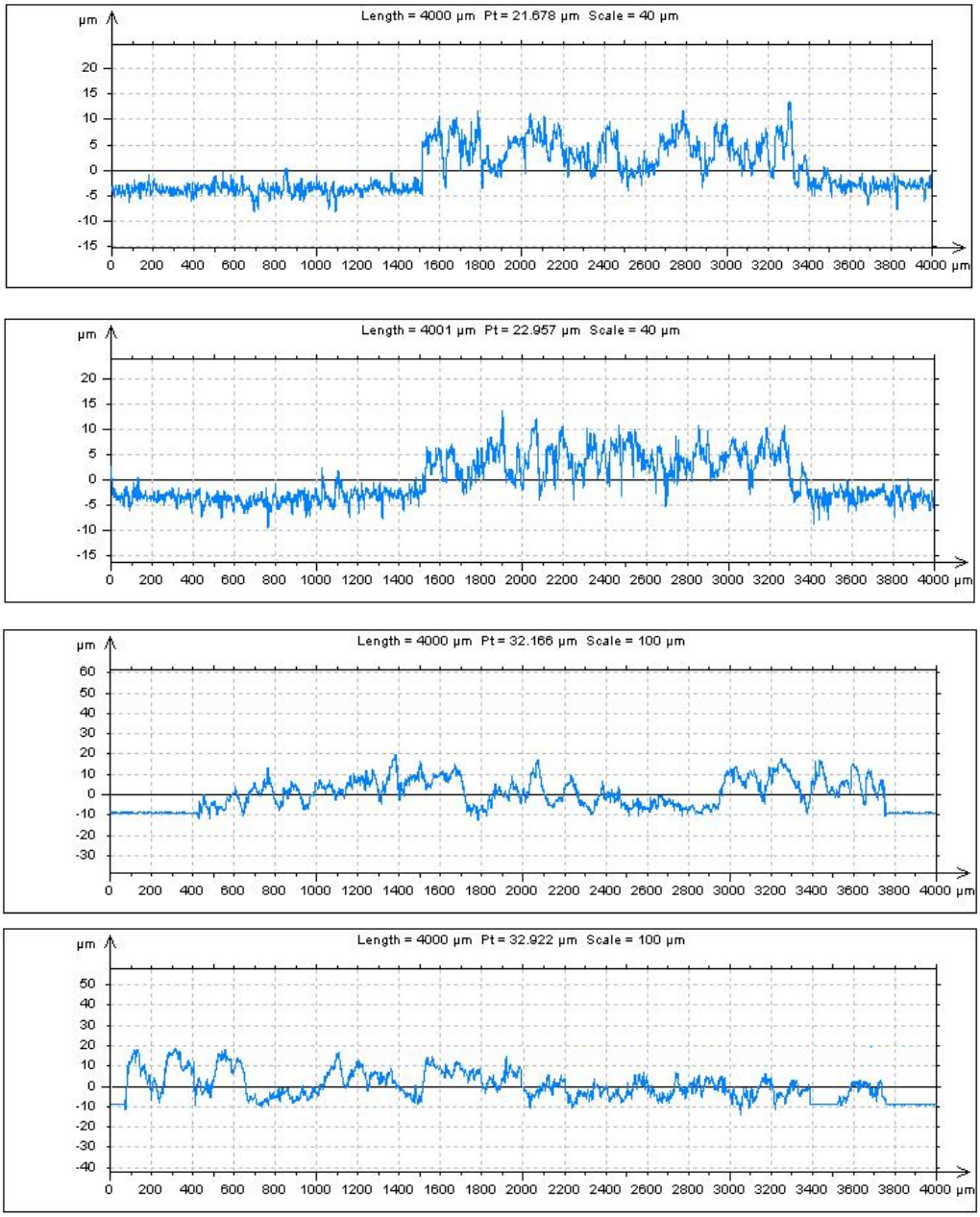

Figure 7 Talysurf profile of a failed adhesive spot on alumina surface, sample 10 top and sample 9 bottom.

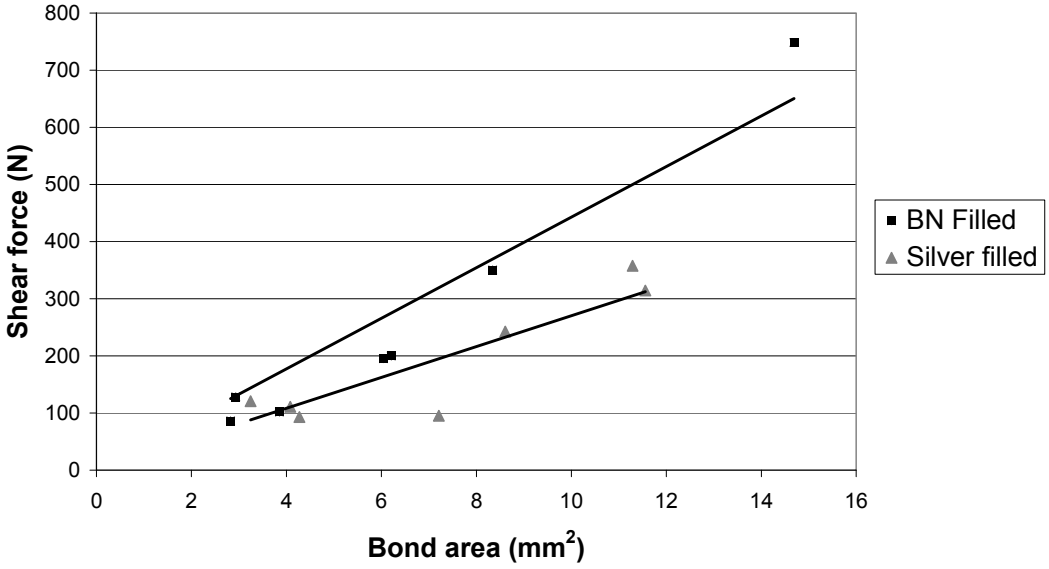

Figure 8 Comparison of bond area to shear force lines are least square best fits with 0 intercept.

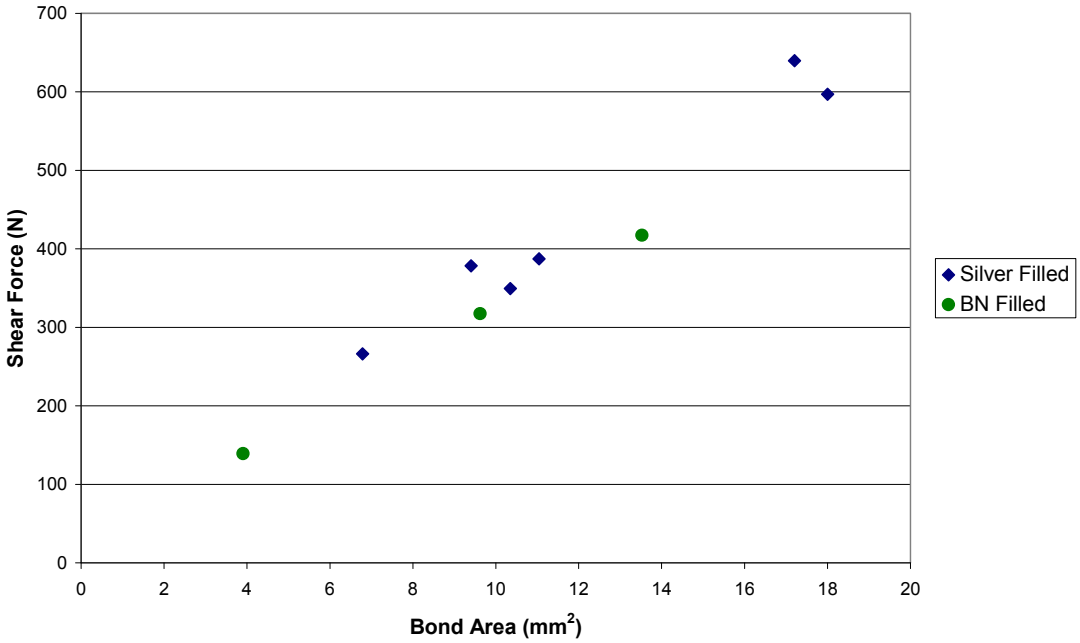

Figure 9 Comparison of bond area to shear force for thermally cycled samples.

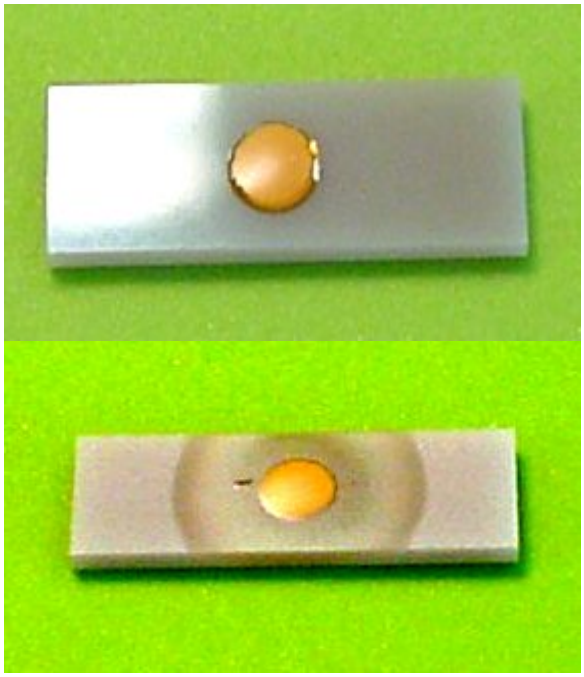

Figure 10 top: minimal epoxy bleed on an AlN polished surface with 20.1% carbon contamination, sample 3. Bottom: pronounced epoxy bleed on an AlN lapped surface with 21.1% carbon contamination, sample 7. Sled lengths are 16mm. Adhesives are boron nitride filled in both cases.

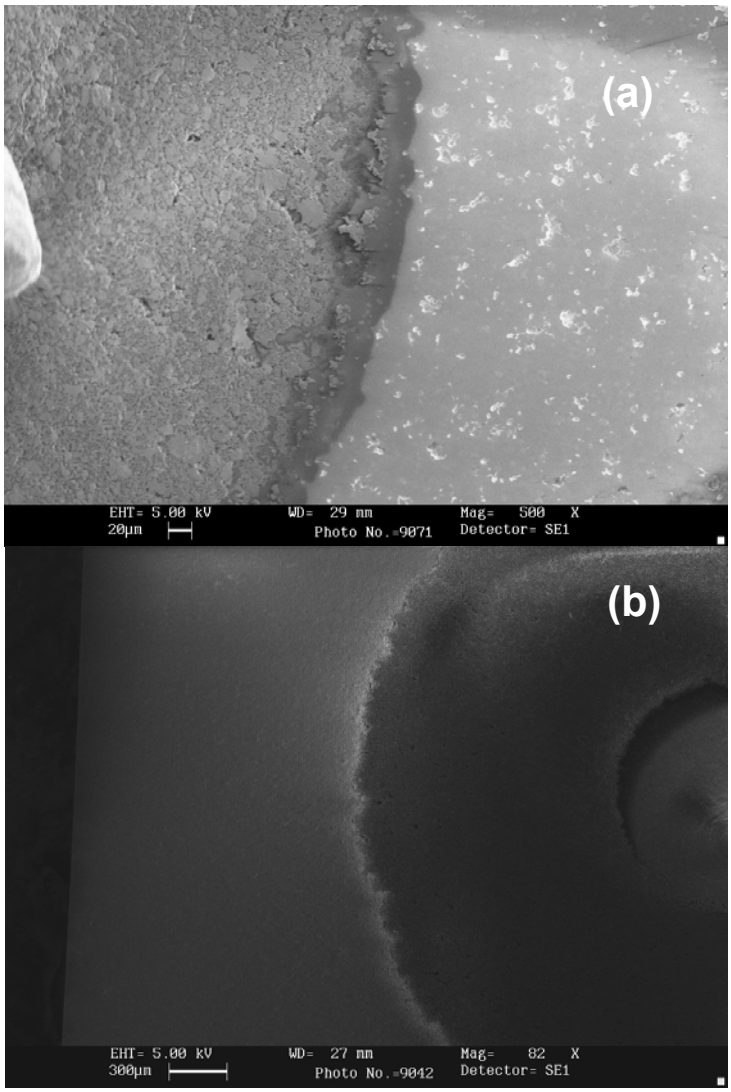

Figure 11 (a) SEM image of limited epoxy bleed on a polished Al_2O_3 surface with 21.2% carbon, sample 9. **(b)** SEM Image of maximum bleed seen with the silver filled adhesive on AlN surface with 21.1% carbon, sample 7.

.

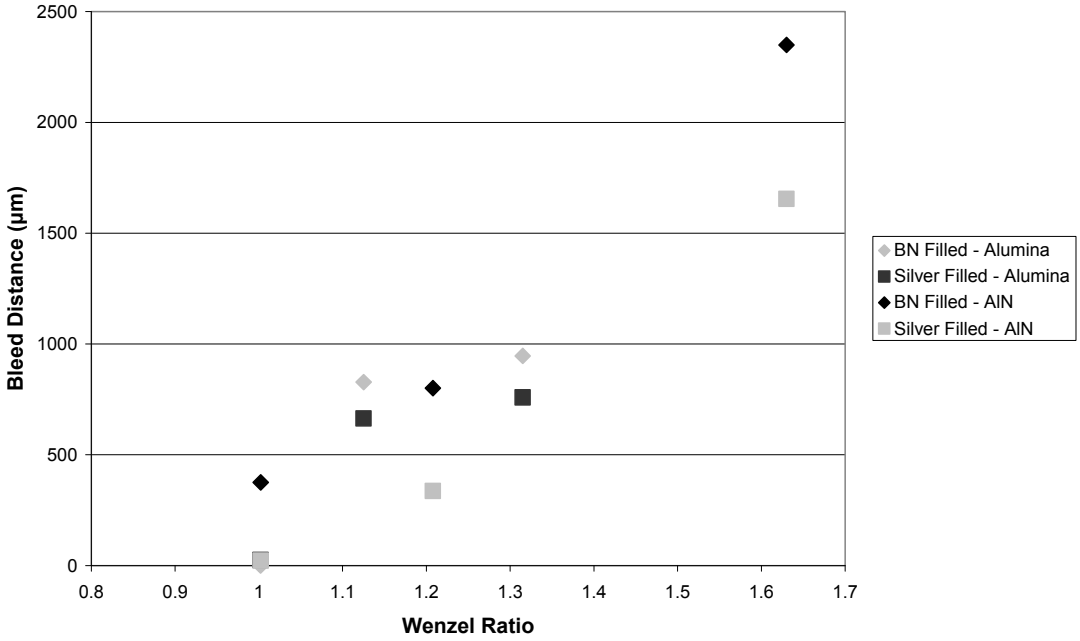

Figure 12 Graph showing the relationship between epoxy bleed distance and Wenzel ratio for plasma cleaned AlN and Alumina with the boron nitride filled and silver filled adhesives.

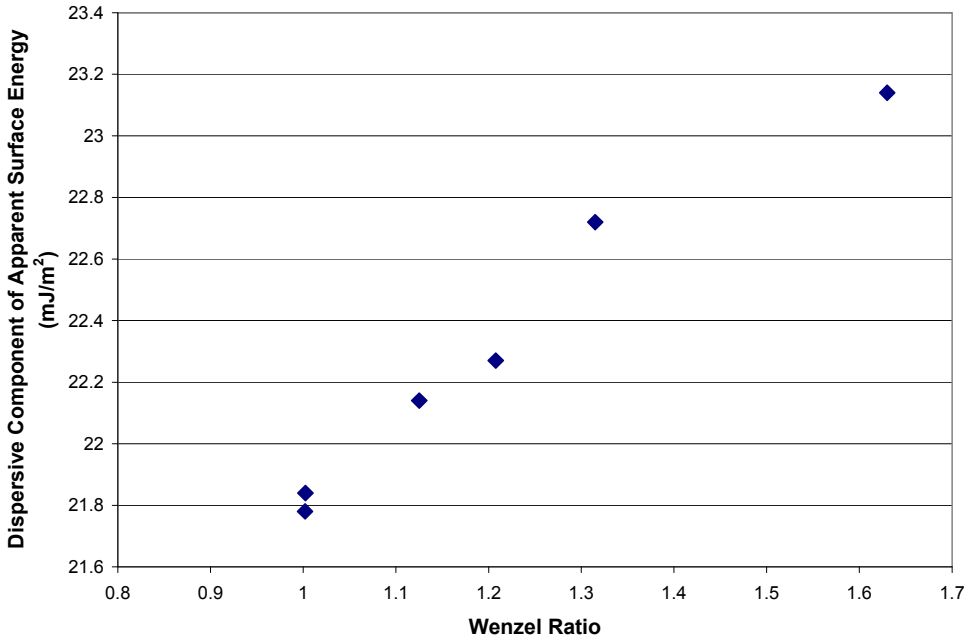

Figure 13 A graph to show the relationship between Wenzel ratio and the dispersive component of apparent surface energy.